Pis'ma v ZhETF, vol. 102, iss. 9, pp. 678 – 682

Suppression of hole relaxation in small-sized Ge/Si quantum dots

A. I. Yakimov[+*1)], *V. V. Kirienko*[+], *A. A. Bloshkin*[+×], *V. A. Armbrister*[+], *A. V. Dvurechenskii*[+×]

[+] *Rzhanov Institute of Semiconductor Physics SB of the RAS, 630090 Novosibirsk, Russia*

[*] *Tomsk State University, 634050 Tomsk, Russia*

[×] *Novosibirsk State University, 630090 Novosibirsk, Russia*

Submitted 10 September 2015

We study the effect of quantum dot size on the mid-infrared photocurrent, photoconductive gain, and hole capture probability in ten-period p-type Ge/Si quantum dot heterostructures. The dot dimensions is varied by changing the Ge coverage during molecular beam epitaxy of Ge/Si(001) system in the Stranski–Krastanov growth mode while keeping the deposition temperature to be the same. A device with smaller dots is found to exhibit a lower capture probability and a higher photoconductive gain and photoresponse. The integrated responsivity in the mid-wave atmospheric window ($\lambda = (3{-}5)\,\mu$m) is improved by a factor of about 8 when the average in-plane dot dimension changes from 18 to 11 nm. The decrease of the dot size is expected to reduce the carrier relaxation rate due to phonon bottleneck by providing strong zero-dimensional quantum mechanical confinement.

DOI: 10.7868/S0370274X15210055

It is well known that quantum dot (QD) infrared photodetectors (QDIPs) have important advantages over quantum well devices. One figure of merit that determined the photoconductive gain and hence the QDIP responsivity is the probability that a carrier is captured by a QD after its optical generation. A remarkable property of QDs originated from their discrete energy spectrum is a suppression of carrier relaxation rates due to the phonon bottleneck effect [1, 2]. If the energy separation between discrete quantized levels in the dot is designed such that it exceeds the energy of optical phonons, then the electron-phonon scattering becomes strongly quenched leading to a long carrier relaxation time. A reduced capture probability of photoexcited carriers will result in enhancement of the photoconductive gain and detector response [3]. Clearly, this effect can be particular important in heterostructures with small QDs having markedly separated bound states.

The phonon bottleneck has been proposed for electrons [1, 2] and observed experimentally for undoped [4–6] and n-type QDs [7, 8] using photoluminescence spectroscopy or pump-probe technique. So far, little attention has been paid to QDIPs with p-type hole response. The attractive features of p-QDIPs include a well-preserved spectral profile [9], as an opposite to a conventional n-type response strongly dependent on applied bias, increased density of states, and lower dark current due to the higher hole effective mass [10]. All these features have motivated the study of the hole capture process in p-type QDs. The work described here focuses on the Ge/Si(001) system. The 4 % lattice mismatch between the Ge epitaxial film and the Si is used to induce the Stranski–Krastanov growth mode where the two-dimensional growth regime changes into a three-dimensional one after the deposition of about 4.5 monolayers of Ge. The Ge/Si QDIPs operate in the mid-infrared atmospheric window by photoexcitation of holes out of Ge QDs into the continuum above the Si barriers and subsequent transportation by an internal or built-in electric field [11–14]. To trace the phonon bottleneck effect we compare detailed measurements of the intraband photocurrent, the photoconductive gain, and the hole capture probability of two Ge/Si QDIPs with Ge dots of different sizes.

Fig. 1a shows schematically the structure of the devices discussed in this paper. The samples were grown by solid source molecular beam epitaxy on a (001) oriented boron doped p^+-Si substrate with resistivity of 0.01 Ω cm. The active region of the devices was composed of ten stacks of Ge quantum dots grown at 500 °C and separated by 35-nm Si barriers. Each Ge layer was formed subsequently by depositing 7 monolayers pure Ge to grow large Ge dots. To grow small Ge dots, the Ge growth in each layer was stopped just after appearance of well-defined three-dimensional spots in the reflection high-energy electron diffraction pattern. The scanning tunneling microscopy (STM) of samples without the Si cap layers was employed to assess the

[1)] e-mail: yakimov@isp.nsc.ru

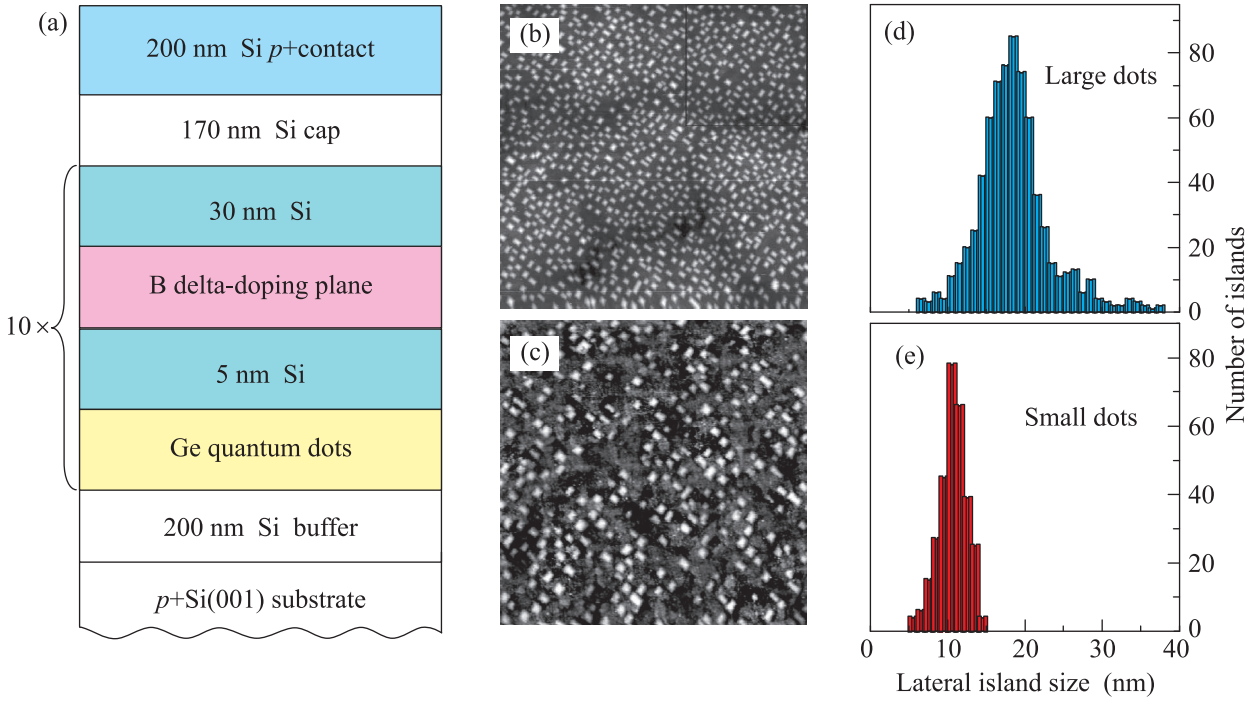

Fig. 1. (Color online) (a) – Layer sequence of the Ge/Si heterostructures. $400 \times 400\,\text{nm}^2$ STM images (b and c) and size distribution histograms (d and e) from topmost uncapped Ge layer of large-dot (b and d) and small-dot (c and e) samples

morphology of the Ge surface (Fig. 1b and c). At the growth temperature used, hut shaped islands are commonly observed. The large Ge dots have a typical base length $\langle l \rangle = 18.2 \pm 3.1$ nm (Fig. 1d), about 2 nm height, and an areal density of $1.1 \cdot 10^{11}\,\text{cm}^{-2}$. For small dots, $\langle l \rangle = 10.8 \pm 1.6$ nm (Fig. 1e), ~ 1 nm height, and a slightly larger density of $1.3 \cdot 10^{11}\,\text{cm}^{-2}$. The active region was sandwiched in between the 200-nm-thick intrinsic Si buffer and cap layers. Finally, a boron doped 200-nm-thick p^+-Si top contact layer was deposited. The p-type remote doping of the dots was achieved with a boron δ-doping layer inserted 5 nm above each dot layer. The areal doping density ($10^{12}\,\text{cm}^{-2}$) was the same for both samples. The Si barriers were deposited at 500 °C before δ-doping and at 600 °C after formation of a boron δ-doping plane. The average Ge content of $x = 0.61$ in large QDs and 0.65 in small dots were determined from Raman scattering experiments (Fig. 2) using an approach described in [15].

For vertical photocurrent (PC) measurements the samples were processed in the form of circular mesas with diameter 4.5 mm by using plasma etching and contacted by Al:Si metallization (the Al/Si spots are about 1 mm in diameter). The bottom contact is defined as the ground when applying voltage to the detectors. The normal-incidence photoresponse was obtained using a Bruker Vertex 70 Fourier transform infrared (FTIR) spectrometer with a spectral resolution of $10\,\text{cm}^{-1}$ along with a SR570 low noise current preamplifier. The PC spectra were calibrated with a deuterated L-alanine doped triglycine sulfate (DLaTGS) detector. The noise characteristics were measured with an SR770 fast Fourier transform analyzer and the white noise region of the spectra was used to determine the gain. The sample noise was obtained by subtracting the preamplifier-limited noise level from the experimen-

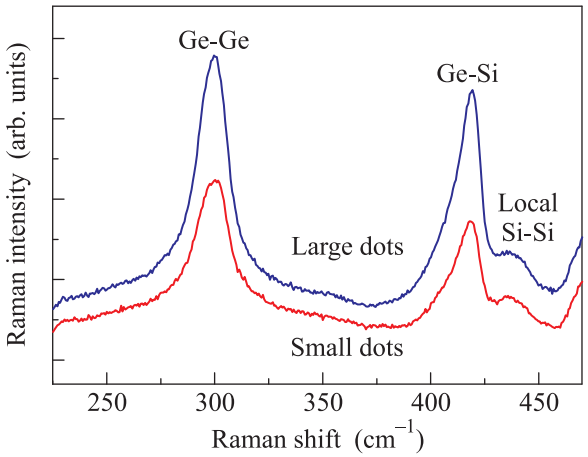

Fig. 2. (Color online) Raman spectra of the samples under study

tal data. The dark current was tested as a function of bias (U_b) by a Keithley 6430 Sub-Femtoamp Remote SourceMeter. The devices were mounted in a cold finger inside a Specac cryostat with ZnSe windows. For dark current and noise measurements, the samples were surrounded with a cold shield. All measurements were carried out at a temperature of 80 K.

Fig. 3 depicts the PC spectra measured at a zero bias voltage in the large-dot and small-dot samples.

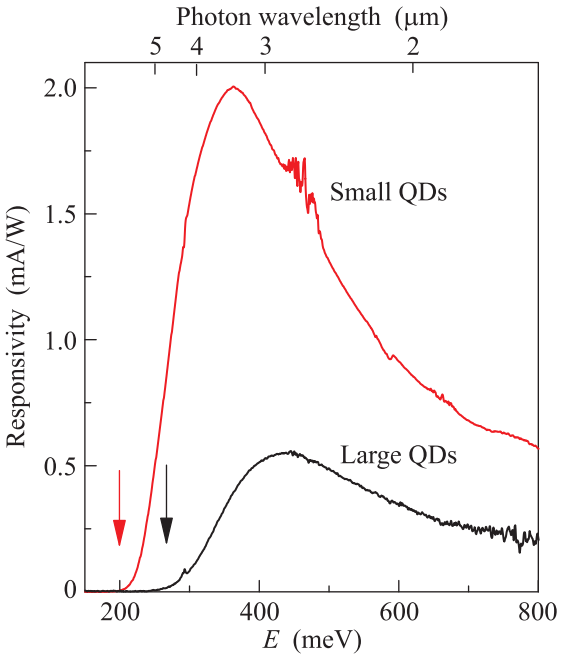

Fig. 3. (Color online) Zero-bias photoresponse measured for the samples with small and large QDs. The arrows indicate the calculated ground-state hole binding energies

Both QDIPs show pronounced photovoltaic behavior caused by a built-in electric field of charged δ-doping planes [14, 16]. The broad nature of the photoresponse suggests that the photocurrent is associated with a bound-to-continuum transition [14, 17, 18]. As the dot size decreases, the peak position shifts toward less photon energy by ~ 100 meV. This property follows directly from the general properties of quantum dots: decreasing the dot dimensions will reduce the hole binding energies getting them closer to the continuum states [19]. We find that the PC for small dots integrated over the mid-infrared atmospheric window from 3 to 5 μm exceeds the signal from large QDs by a factor of about 8.

In order to support the origin of photoresponse, we performed a three-dimensional analysis of the valence band diagram for the samples under study. For a simulation of electronic structure, we considered a pyramidal Ge_xSi_{1-x} nanocluster with four {105}-oriented facets and a (001) base embedded into the Si matrix. The nanocluster composition x was taken from analysis of Raman data. The pyramid lies on a thin Ge_xSi_{1-x} wetting layer. The finite element calculations of three-dimensional spatial distribution of strain components $\varepsilon_{\alpha\beta}$ were performed using the package COMSOL Multiphysics with the approach described in [20]. The strain tensor elements were subsequently used as input to a strain-dependent Hamiltonian. The hole energy spectra were calculated with a six-band $\mathbf{k}\cdot\mathbf{p}$ approximation (three valence bands and spin), based on the method of Bir and Pikus [21], which includes spin-orbit and strain effects. Details of the model and formulation can be found in [22]. From theoretical analysis, we found that the ground hole state is located about 270 and 200 meV from the Si barrier edge for the large-dot and small-dot samples, respectively. Both these values agree well with the onset of the photoresponse shown by arrows in Fig. 3. Thus, the observed photocurrent is associated with the dominant transitions from the ground state within the Ge dots to continuum states at the Si valence band edge. Possible optical excitations from the other bound states have much smaller oscillator strength due to the presence of the nodal planes in wavefunction density and make a small contribution to PC.

Fig. 4 compares the peak responsivity R of two devices, which shows a significant improvement of R over

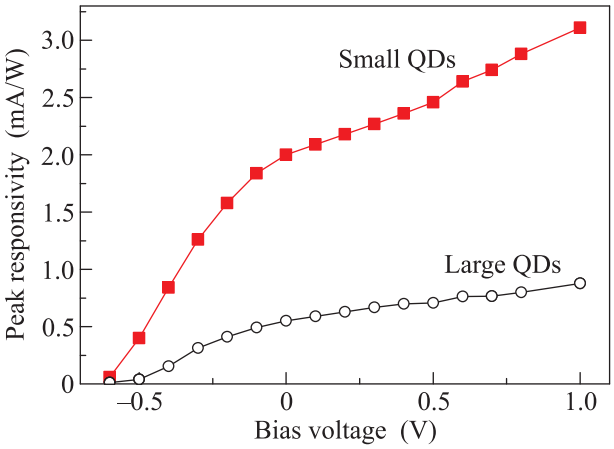

Fig. 4. (Color online) Peak responsivity as a function of applied bias for QDIPs with small and large QDs

the wide bias range: the peak photoresponse of the sample with small dots is found to be about 4 times higher than that of the large-dot sample. The data were taken at $E_{\text{peak}} = 363$ meV ($\lambda = 3.4\,\mu$m) for sample with small QDs and at $E_{\text{peak}} = 432$ meV ($\lambda = 2.9\,\mu$m) for sample with large QDs. Asymmetry of $R(U_b)$ dependence with respect to zero bias is a typical feature of Ge/Si

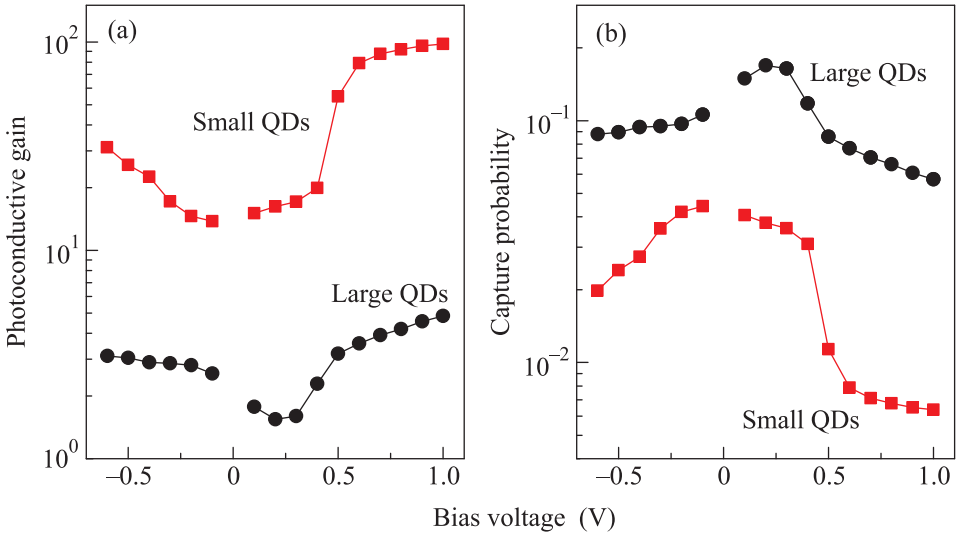

Fig. 5. (Color online) Photoconductive gain (a) and hole capture probability (b) as a function of applied bias

QDIPs with a remote delta-doping of Si barriers and has been discussed in detail in [14]. Responsivity is given by $R = (e\lambda/hc)\eta g$, where c is the speed of light, η is the absorption quantum efficiency, and g is the photoconductive gain defined as the ratio of the photocarrier lifetime over the transit time. Since the dot density and doping level are approximately the same in both samples, we suggest that the rise of R is primarily due to increased photoconductive gain.

From noise measurements, we established that the noise level at finite bias is dominated by a generation-recombination noise. In this case, when the carrier capture probability into a QD is small, the gain is given by

$$g = i_n^2/(4eI_d\Delta f), \tag{1}$$

where e is the charge of an electron, i_n is the noise current, I_d is the dark current, and Δf is the noise bandwidth. From the other hand, the gain can be expressed in terms of the capture probability of an electron (or hole) traversing a QD layer p_c as [23]

$$g = \frac{1 - p_c/2}{FNp_c}, \tag{2}$$

where F is the fill factor which describes the area coverage of the QDs in a dot layer, N is the number of QD layers. The fill factor of 0.35 and 0.16 was estimated from STM data presented in Fig. 1b and c, respectively. For the evaluation of the gain, we have subtracted the thermal (Johnson) noise from the measured noise in order to have the pure generation-recombination noise. The Johnson noise was calculated as $i_{\text{J}} = \sqrt{4kT\Delta f/\rho}$, where k is the Boltzmann's constant, T is the temperature, and ρ is the differential resistance, which is extracted from the dark current measurements.

The gain and hole capture probability calculated using Eqs. (1) and (2) are shown in Fig. 5. For the sample with small QDs, the gain is much higher than unity and the capture probability is small displaying a suppression factor of 2.5 to 10 depending on applied voltage. Reduction of the hole capture probability, enhancement of photocurrent and gain with the decrease of dot size can be explained if we assume a phonon bottleneck effect for holes. The calculated energy gaps between the ground and the first excited state are $\Delta E = 37$ and 60 meV for the samples containing large and small QDs, respectively. The energy level spacing for the small Ge dots exceeds all LO phonon energies corresponding to Si–Si (54 meV), Si–Ge (52 meV), and Ge–Ge (37 meV) vibrations (Fig. 2) and therefore holes can display an effective bottleneck in the relaxation toward the ground state due to the lack of phonons needed to satisfy the energy conservation rule. An opposite energy ratio is observed for the large dots where the Si–Si and Si–Ge phonon energies are larger than ΔE and the Ge–Ge energy is very close to ΔE. In this case the single-phonon mediated scattering process becomes allowed due to interaction with a Ge–Ge vibration mode, in agreement with the experimental observations. We emphasize here that since only holes (i.e., no electrons) are involved in experiment, the electron-hole interaction [24] and Auger-assisted relaxation [25] are not expected to dominate.

In summary, we have studied the impact of QD size on the photoelectrical characteristics of p-type Ge/Si quantum-dot heterostructures. In particular, we obtain an improvement of the peak responsivity by a factor

of 4 by enhancing the photoconductive gain due to the phonon bottleneck effect, which we realize by reducing the dot dimensions. Our results indicate that a proper choice of QD size can serve as a promising way to optimize the Ge/Si QDIP performance.

The authors are much obliged to V.A. Volodin for Raman measurements. The work was funded by Russian Scientific Foundation (grant # 14-12-00931).

1. U. Bockelmann and G. Bastard, Phys. Rev. B **42**, 8947 (1990).
2. H. Benisty, C. M. Sotomayor-Torrés, and C. Weisbuch, Phys. Rev. B **44**, 10945 (1991).
3. V. Ryzhii, I. Khmyrova, V. Pipa, V. Mitin, and M. Willander, Semicond. Sci. Technol. **16**, 331 (2001).
4. T. Kitamura, R. Ohtsubo, M. Murayyama, T. Kuroda, K. Yamaguchi, and A. Tackeuchi, Phys. Stat. Sol. (c) **0**, 1165 (2003).
5. J. Urayama, T. B. Norris, J. Singh, and P. Bhattachara, Phys. Rev. Lett. **86**, 4930 (2001).
6. G. Reithmaier, F. Flassig, P. Hasch, S. Lichtmannecker, K. Müller, J. Vǔcković, R. Gross, M. Kaniber, and J. J. Finley, Appl. Phys. Lett. **105**, 081107 (2014).
7. S. Sauvage, P. Boucaud, R. P. S. Lobo, F. Bras, G. Fishman, G. Prazeres, F. Glotin, J. M. Ortega, and J.-M. Gèrard, Phys. Rev. Lett. **88**, 177402 (2002).
8. E. A. Zibik, L. R. Wilson, R. P. Green, G. Bastard, R. Ferreira, P. J. Phillips, D. A. Carder, J.-P. R. Wells, J. W. Cockburn, M. S. Skolnick, M. J. Steer, and M. Hopkinson, Phys. Rev. B **70**, 161305(R) (2004).
9. Y.-F. Lao, S. Wolde, A. G. Unil Perera, Y. H. Zhang, T. M. Wang, J. O. Kim, T. Schuler-Sandy, Z.-B. Tian, and S. S. Krishna, Appl. Phys. Lett. **104**, 171113 (2014).
10. Y.-F. Lao, S. Wolde, S. Wolde, A. G. Unil Perera, Y. H. Zhang, T. M. Wang, H. C. Liu, J. O. Kim, T. Schuler-Sandy, Z.-B. Tian, and S. S. Krishna, Appl. Phys. Lett. **103**, 241115 (2013).
11. C. Miesner, O. Röthig, K. Brunner, and G. Abstreiter, Appl. Phys. Lett. **76**, 1027 (2000).
12. C.-H. Lin, C.-Y. Yu, C.-Y. Peng, W. S. Ho, and C. W. Liu, J. Appl. Phys. **101**, 033117 (2007).
13. E. Finkman, N. Shuall, A. Vardi, V. Le Thanh, and S. E. Schacham, J. Appl. Phys. **103**, 093114 (2008).
14. A. I. Yakimov, V. A. Timofeev, A. A. Bloshkin, V. V. Kirienko, A. I. Nikiforov, and A. V. Dvurechenskii, J. Appl. Phys. **112**, 034511 (2012).
15. A. I. Yakimov, A. I. Nikiforov, A. V. Dvurechenskii, V. V. Ulyanov, V. A. Volodin, and R. Groetzschel, Nanotechnology **17**, 4743 (2006).
16. L. Chu, A. Zrenner, G. Böhm, and G. Abstreiter, Appl. Phys. Lett. **75**, 3599 (1999).
17. D. Pan, E. Towe, and S. Kennerly, Appl. Phys. Lett. **73**, 1937 (1998).
18. A. D. Stiff, S. Krishna, P. Bhattacharya, and S. Kennerly, Appl. Phys. Lett. **79**, 421 (2001).
19. N. A. Ameen and Y. M. El-Batawy, J. Appl. Phys. **113**, 193102 (2013).
20. S. Christiansen, M. Albrecht, and H. P. Strunk, Appl. Phys. Lett. **64**, 3617 (1994).
21. G. L. Bir and G. E. Pikus, *Symmetry and Strain-Induced Effects in Semiconductors*, Wiley, N.Y. (1974).
22. A. I. Yakimov, A. A. Bloshkin, and A. V. Dvurechenskii, Phys. Rev. **81**, 115434 (2010).
23. Z. Ye, J. C. Campbell, Z. Chen, E. T. Kim, and A. Madhukar, Appl. Phys. Lett. **83**, 1234 (2003).
24. U. Bockelmann, Phys. Rev. B **48**, 17637 (1993).
25. U. Bockelmann and T. Egeler, Phys. Rev. B **46**, 15574 (1992).